JOURNAL OF GEOPHYSICAL RESEARCH: ATMOSPHERES, VOL. 118, 6750–6763, doi:10.1002/jgrd.50490, 2013

Pollutant transport among California regions

Wayne M. Angevine,[1,2] Jerome Brioude,[1,2] Stuart McKeen,[1,2] John S. Holloway,[1,2] Brian M. Lerner,[1,2] Allen H. Goldstein,[3] Abhinav Guha,[3] Arlyn Andrews,[2] John B. Nowak,[1,2] Stephanie Evan,[1,2] Marc L. Fischer,[4] Jessica B. Gilman,[1,2] and Daniel Bon[1,2,5]

Received 19 November 2012; revised 7 March 2013; accepted 12 March 2013; published 20 June 2013.

[1] Several regions within California have significant air quality issues. Transport of pollutants emitted in one region to another region may add to the impact of local emissions. In this work, Lagrangian particle dispersion model simulations show the amounts of tracers that are transported within and among four regions, Southern California, the San Francisco Bay Area, the Central Valley, and the rest of the state. The simulations cover May and June of 2010, the California Research at the Nexus of Air Quality and Climate Change experiment period. Tracers of automobile emissions and one type of agricultural emission are used. Tracer mixing ratios are compared to airborne and ground-based measurements. The age of tracers in each location is also presented. Vertical profiles and diurnal cycles help to clarify the transport process. As is well known, Southern California emissions are transported to the east and affect the desert areas, and Bay Area automobile emissions are an important source of pollutants in the San Joaquin Valley. A novel result is that the Southern California Bight is filled with a mixture of well-aged carbon monoxide tracer from Southern California and the Bay Area. Air over the Bight is also affected by the agricultural emissions represented by the agricultural tracer, dominantly from the Central Valley where its sources are largest. There is no indication of transport from Southern California to the Central Valley. Emissions from the Central Valley do make their way to Southern California, as shown by the agricultural tracer, but automobile emissions from the Valley are insignificant in Southern California.

Citation: Angevine, W. M., et al. (2013), Pollutant transport among California regions, *J. Geophys. Res. Atmos.*, *118*, 6750–6763, doi:10.1002/jgrd.50490.

1. Introduction

[2] California is a large state with several distinct regions (Figure 1), some of which have air quality problems. Air quality within each region (for example, Southern California) has been extensively studied. Less attention has been given to the possible impacts of one region on others. It is known that pollution produced in the Los Angeles area is transported eastward to the deserts [*Langford et al.*, 2010; *Riley et al.*, 2008; *White and Macias*, 1990] and that pollutants from the San Francisco Bay Area affect the Central Valley and the foothills of the Sierra Nevada [*Bao et al.*, 2008; *Beaver and Palazoglu*, 2009; *Michelson and Bao*, 2008; *Riley et al.*, 2008]. Other possible interregional impacts are from Southern California and the Bay Area to the coastal waters and from the Central Valley to the mountains, deserts, and Southern California. Transport between and within regions takes place in the free troposphere as well as in the boundary layer [*Neuman et al.*, 2012].

[3] Upwind regions contribute to pollution within California [*Cooper et al.*, 2011; *Langford et al.*, 2012; *Neuman et al.*, 2012]. *Pfister et al.* [2011] recently examined the sources of carbon monoxide (CO) in California using an online chemistry model. Their emphasis was on inflow and wildfires, and they treated all California CO emissions as one tracer. Here we examine the complementary question of transport within California by distinguishing among tracer emissions from California regions. We consider both automobile CO emissions and one type of agricultural emissions (NH_3), which have quite different spatial patterns.

[4] The tool used here is a Lagrangian particle dispersion model, FLEXPART, driven by a mesoscale meteorological model, Weather Research and Forecast (WRF). FLEXPART is run forward in time, transporting specified tracer emissions. Details of the models are given in section 2.

[5] Data from the 2010 California Research at the Nexus of Air Quality and Climate Change (CalNex) field study [*Ryerson et al.*, 2013] are used to evaluate the simulations and reinforce the results. CalNex was conducted in May–July

Additional supporting information may be found in the online version of this article.

[1]Cooperative Institute for Research in Environmental Sciences, University of Colorado Boulder, Boulder, Colorado, USA.
[2]NOAA Earth System Research Laboratory, Boulder, Colorado, USA.
[3]Department of Environmental Science, Policy, and Management, University of California, Berkeley, California, USA.
[4]Lawrence Berkeley National Laboratory, Berkeley, California, USA.
[5]Now at Colorado Department of Public Health and Environment, Denver, Colorado, USA.

Corresponding author: W. M. Angevine, NOAA ESRL R/CSD4, 325 Broadway, Boulder, CO 80305, USA. (Wayne.M.Angevine@noaa.gov)

2169-897X/13/10.1002/jgrd.50490

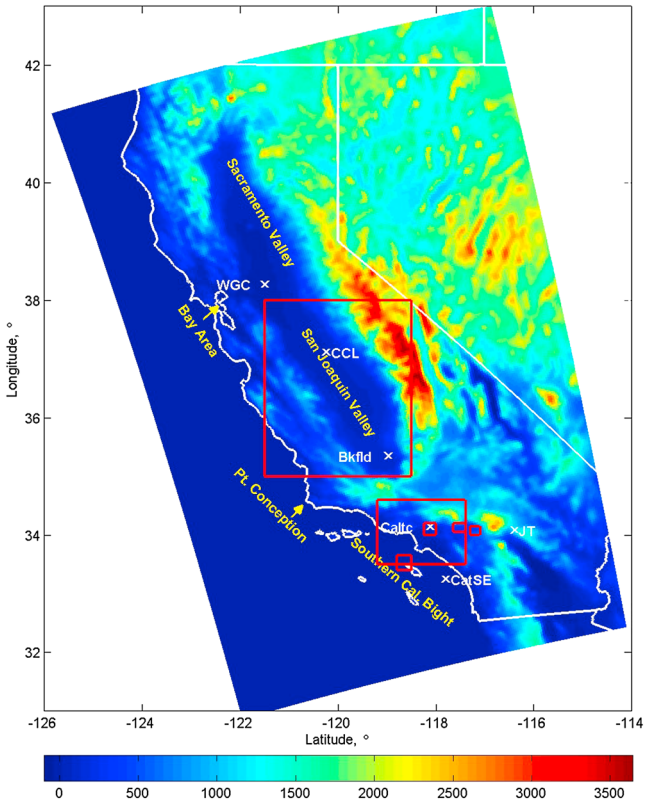

Figure 1. Terrain elevation (m) of California with regions (red boxes), sites (white text and cross marks), and general areas (yellow text) referred to in the text and figures. Large northern region is "San Joaquin," large southern region is "LA basin." Small regions, left to right, are "Catalina," "Pasadena," "Fontana," and "Redlands." Sites are Walnut Grove (WGC), Chowchilla (CCL), Bakersfield (Bkfld), Caltech (Caltc), Joshua Tree (JT), and southeast of Catalina (CatSE).

2010 throughout California, with measurements from several mobile platforms and ground sites. Data from operational measurements are also used.

[6] Uncertainties in the results due to errors in the meteorological model and in emissions cannot be precisely estimated, but are probably large. The results are therefore presented in qualitative terms. Full discussion of uncertainties and their impacts is presented in section 6. The results herein apply only to the late spring and early summer seasons. Patterns in other seasons may be quite different.

2. Model Configurations

2.1. WRF

[7] The WRF model, Advanced Research core (ARW), was used to provide the meteorological fields to drive FLEXPART. WRF was run on nested grids of 36, 12, and 4 km spacing with two-way nesting. *Angevine et al.* [2012] evaluated the performance of several WRF configurations against a variety of data. The FLEXPART runs reported here used their configuration EM4N, which produced the best overall performance. The only important bias found in the evaluation was a general tendency to overestimate wind speeds. Boundary layer heights and vertical mixing were found to be nearly unbiased, and this will be confirmed by the comparisons between P3 CO data and FLEXPART results below. Random errors are substantial but comparable to other studies, and their implications are also discussed below. The EM4N configuration was initialized and provided boundary conditions from the ERA-Interim reanalysis [*Dee et al.*, 2011] and used the Noah land surface model [*Chen and Dudhia*, 2001; *Chen et al.*, 2011] with Moderate Resolution Imaging Spectroradiometer (MODIS) land use and land cover data and the single-layer urban canopy model. Other physics options [*Skamarock et al.*, 2008, and references therein] included Eta microphysics, RRTMG longwave and shortwave radiation, and Grell-Devenyi cumulus (outer

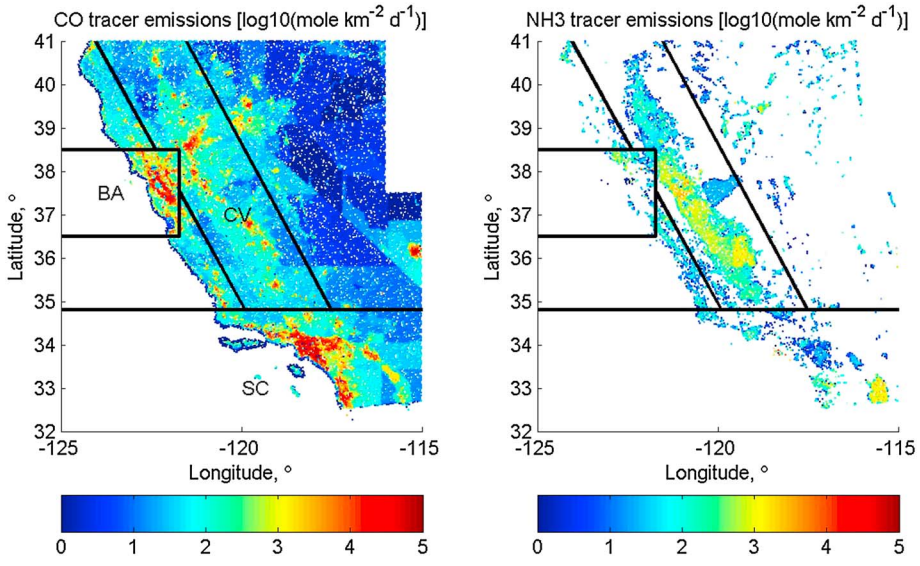

Figure 2. Emissions of automotive (CO, left) and agricultural (NH_3, right) tracers. Black lines mark the four emission regions (Southern California (SC), Bay Area (BA), Central Valley (CV), and Other (OT).

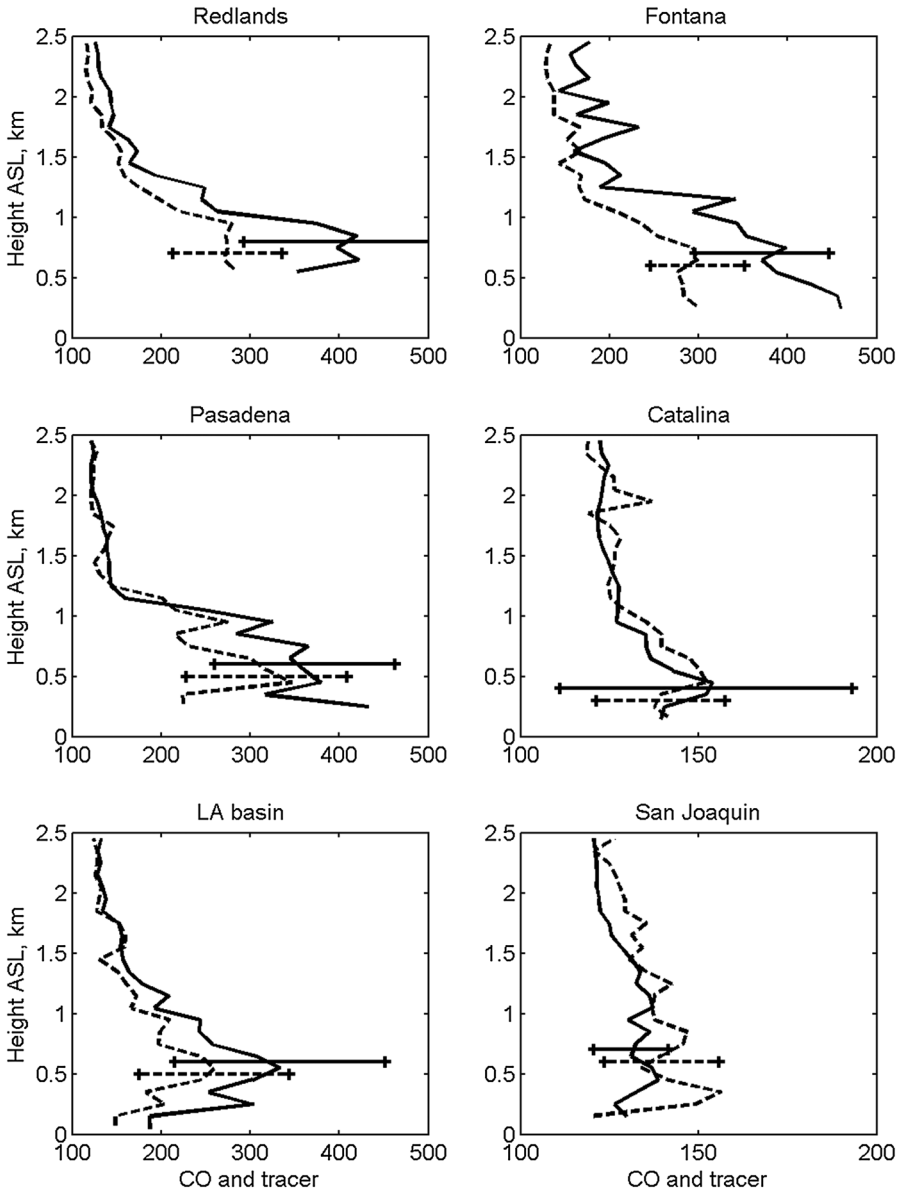

Figure 3. Average profiles of CO (ppb) measured by the NOAA P3 (dashed) and FLEXPART/WRF simulated CO tracer (solid). Assumed background of 120 ppb added to simulated tracer values. Bars are plus and minus one standard deviation at one height for each region.

domain only). The soil was initialized with the ERA-Interim soil temperature and moisture fields without spin-up. Sea surface temperature was the U.S. Navy GODAE high-resolution sea surface temperature (SST) (see http://www.usgodae.org/ftp/outgoing/fnmoc/models/ghrsst/docs/ghrsst_doc.txt) updated every 6 h and interpolated between updates. The vertical grid had 60 levels, 19 below 1 km, lowest level approximately 16 m. Run EM4N used the Mellor-Yamada-Janjic (MYJ) planetary boundary layer (PBL) and surface layer options [*Janjic*, 2002; *Sušelj and Sood*, 2010].

2.2. FLEXPART

[8] We used a version of the FLEXPART Lagrangian particle dispersion model [*Stohl et al*., 2005] modified to use WRF output [*Brioude et al*., 2011; *Fast and Easter*, 2006]. FLEXPART uses the same grid spacing and vertical levels as in WRF. FLEXPART solves turbulent motion in a Lagrangian framework using first-order Langevin equations. The turbulent motion is stochastic and parameterized using the Hanna scheme. The scheme uses PBL height, Monin-Obukhov length, convective velocity scale, roughness length, and friction velocity. The PBL height and friction velocity are read from the WRF output. The PBL height in WRF with the MYJ PBL scheme used here is calculated based on a turbulent kinetic energy threshold. FLEXPART prescribes a turbulent profile based on the Hanna scheme [*Stohl et al*., 2005], depending on convective, neutral, or stable conditions. Here FLEXPART is run forward in time. In forward runs, particles are emitted at the surface and transported by the WRF-simulated winds and a stochastic component. We used the WRF output with an output time interval of 30 min. The number of particles emitted per unit time in each grid square is proportional to the tracer (CO or NH_3) emissions at that time and place in the inventory (described below). Each particle

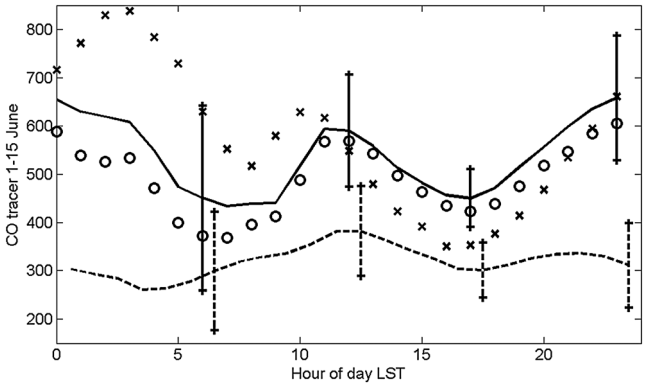

Figure 4. Average diurnal cycle of observed CO (ppb) (dashed) and simulated CO tracer in the lowest model layer (solid) at Caltech ground site for 1–15 June only. Vertical bars are plus and minus one standard deviation at selected hours. Circles are tracer averaged over 0–300 m agl, crosses are tracer simulated with no diurnal cycle of emission. At Caltech, essentially all the CO tracer is from Southern California.

carries a fixed quantity of tracer. The time of emission is carried with each particle. We used time-average wind out of WRF to reduce trajectory uncertainties in a complex terrain region like California [*Brioude et al*., 2012] because time-average wind is more representative of the wind variability than instantaneous wind out of WRF. *Brioude et al*. [2012] have shown that this setup conserves the well-mixed criterion in the PBL in FLEXPART. Above the PBL, a simple coefficient of diffusivity is used to simulate the horizontal turbulent motion in the free troposphere. Particles are not exchanged by turbulence between the PBL and the free troposphere but by horizontal displacement or by the resolved vertical displacement in the WRF wind.

[9] We defined the FLEXPART output grid (which is independent of the grid on which the transport is calculated) with a 4 km grid spacing in both horizontal dimensions and 28 vertical layers, each 100 m thick. The horizontal grid corresponds to that used for the driving WRF simulations.

[10] FLEXPART simulations started at 0000 UTC 2 May 2010 and ended at 0000 UTC 1 July. Approximately 3 million particles were emitted each day of the simulation. Particles were retained until they left the simulation domain. No chemical transformation or deposition was simulated. Particle age was divided into six geometrically increasing bins (<3, 3–6, 6–12, 12–24, 24–48, and >48 h). Average tracer age at each grid point is calculated by a weighted average of the number of particles in each bin. Note that "age" as used here is simply time since emission.

2.3. Emissions

[11] Emissions of two tracer categories, carbon monoxide (CO) from on-road automotive sources and ammonia (NH_3) from livestock operations, are incorporated in the FLEXPART simulations (Figure 2). The basis for the emissions is the 2005 National Emissions Inventory [*U.S. EPA*, 2012] (version 2), hereafter referred to as NEI-05. The complete gridded inventory is available electronically at: ftp://aftp.fsl.noaa.gov/divisions/taq/emissions_data_2005, and a detailed description is provided in *Kim et al*. [2011]. CO emissions have been previously evaluated for southeast Texas [*Brioude et al*., 2011] and Southern California [*Brioude et al*., 2013]. An overestimate of CO emissions from two and four stroke mobile nonroad sources in this early release of the NEI-2005 inventory results in total CO emissions being too high by about a factor of 2 [*Brioude et al*., 2011]. As shown further within [*Brioude et al*., 2013], the NEI-05 mobile on-road CO emissions in Southern California are quite consistent with the mobile CO from the California Air Resources Board estimates, and on-road sources dominate CO emissions within that inventory. For this reason, only the mobile on-road CO sources from NEI-05 are used here. The automotive CO tracer is subdivided into four regional tracers (Figure 2) for Southern California (SC), Bay Area (BA), Central Valley (CV), and Other (OT). The diurnal cycle for light-duty vehicles from *Harley et al*. [2005] was imposed (note that this is different from the NEI-05 diurnal cycle). Saturday, Sunday, and weekday emissions differed according to the proportions of Harley et al., but the diurnal cycle was the same for every day of the week (the weekday cycle was used). Similarly, four "NH_3" tracers imitating agricultural emissions were simulated, with emissions as of NH_3 from livestock and manure from NEI-05. No diurnal cycle was used for these emissions. The OT category included emissions from sources in California outside the other three regions and some emissions from Nevada (Figure 2).

3. Evaluation

[12] Model-data comparisons for several sites and platforms are included here. The comparisons provide a general sense of the fidelity of transport patterns (horizontal and vertical). We do not expect (or find) quantitative agreement for several reasons, including inventory uncertainty and other uncertainties discussed in section 6. One specific factor is that the CO tracer includes only on-road sources (see

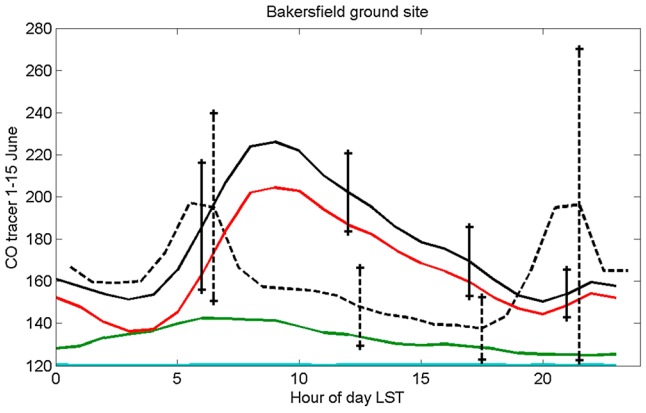

Figure 5. Average diurnal cycle of observed CO (ppb) (dashed) and simulated CO tracers (solid and colors) at Bakersfield ground site. Vertical bars are plus and minus one standard deviation of the observations and total CO tracer at selected hours. For this and similar figures, tracers are total (solid black), Southern California (blue), Bay Area (green), Central Valley (red), and Other (cyan). Southern California and Other are negligible at Bakersfield. Assumed CO background of 120 ppb has been added to the tracers.

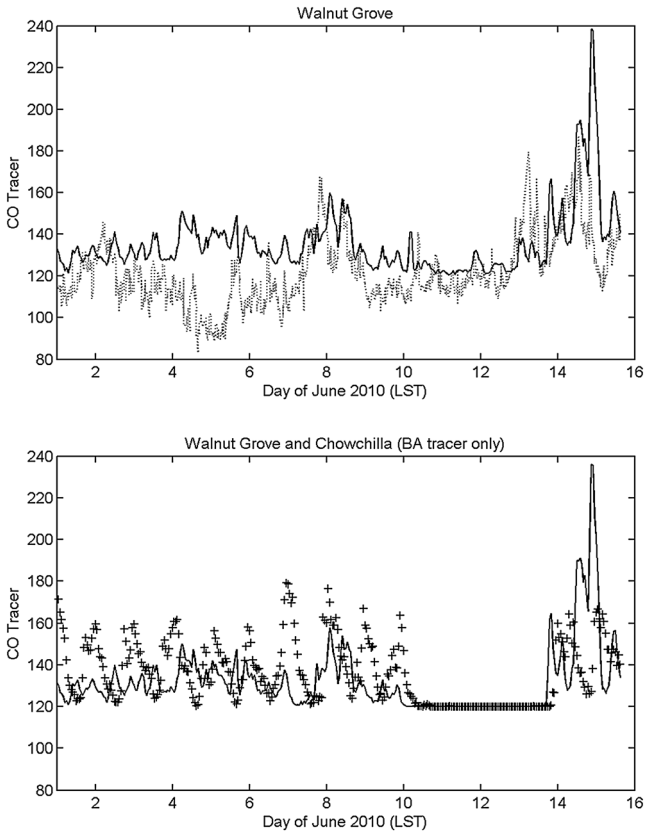

Figure 6. Time series of (top) measured CO (dotted) and simulated CO (all tracers, solid) at the lowest measurement level (31 m agl) and lowest model layer at Walnut Grove, and (bottom) Bay Area CO tracer at Walnut Grove (solid) and Chowchilla (plus signs). Assumed background of 120 ppb has been added to the tracers.

section 2.3 above). Another important issue is the background value of CO, since the simulations only include regional sources and not all of those. This is a research question in itself, starting with the definition of "background." Measurements at Trinidad Head (on the northern California coast) by NOAA Global Monitoring Division (available at http://www.esrl.noaa.gov/gmd/dv/iadv/) show rapidly changing values during May and June at this upwind, primarily marine site. Below we assume a CO background value of 120 ppb for purposes of these comparisons only. Figure 1 shows part of the WRF/FLEXPART domain with regions and locations used for evaluation marked. Measured CO profiles from the NOAA WP3 aircraft are compared with the simulated profiles in Figure 3. The profiles are matched in time and space and averaged over all points within the boxes shown in Figure 1, and in 100 m height bins. All 19 P3 flights (4 May through 22 June) are included, although not all flights contribute data to all boxes. A minimum of 40 one-second samples are required for a bin to be shown. The number of samples per bin varies considerably, the best sampling being in the middle heights (approximately 400–1000 m above ground level (agl)). These profiles should not be interpreted as mean profiles of CO for those locations, since they are strongly influenced by sampling due to purposeful flight planning. The profiles indicate a general overestimation by the model except in the San Joaquin Valley. The vertical structure, however, is very well simulated. The assumed background of 120 ppbv for these regions is supported by the good agreement at the upper levels of the profiles. The standard deviation bars show that the modeled and measured variability at the well-sampled levels is comparable (roughly proportional to magnitude) except at Catalina, where the simulation is much more variable, probably due to the missing clouds in the model, and at San Joaquin, where the measurement is more variable.

[13] The average diurnal cycle of measured CO and simulated tracer at the Caltech ground site are shown in Figure 4. The simulation overestimates at all times of day, most severely at night. The shape of the daytime portion of the cycle is well simulated, with a midday peak due to transport from polluted areas south and southwest of the site. The overestimation at night is due to a combination of faster wind speeds, lower (or less mixed) boundary layers than in reality, and overestimated emissions. Faster wind speeds (shown by *Angevine et al.* [2012]) lead to more efficient transport of tracer from the areas of strong emission in and around downtown Los Angeles. The variability (standard deviation) of simulation and measurement is similar at all times, which, taken together with the larger magnitude in the simulation, indicates proportionally less variability. When the diurnal cycle of emissions is removed (also shown in Figure 4), the nighttime overestimation is much more severe, the midday peak is shifted earlier, and concentrations in the afternoon are reduced. Thus, we see that correct simulation of the diurnal cycle at Caltech depends on a correct cycle of emissions as well as correct transport and mixing. The diurnal cycle does not depend strongly on what model layers are included, as shown by the 0–300 m average line in the figure.

[14] At the Bakersfield ground site (Figure 5), an overestimation of tracer concentration is also seen. The diurnal cycle is poorly simulated. The morning and evening peaks of measured CO could be due to a diurnal cycle of real emissions that differs from what we used in the simulations,

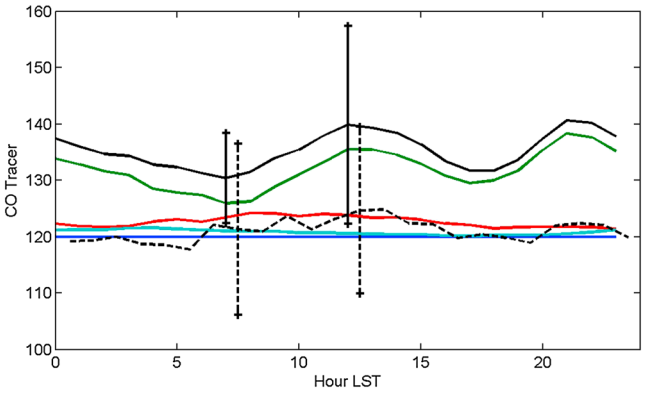

Figure 7. Average diurnal cycle of observed CO (ppb) (dashed) and simulated tracers (solid and colors) at the Walnut Grove tall tower site. Vertical bars are plus and minus one standard deviation of the observations and total CO tracer at selected hours. For this and similar figures, tracers are total (solid black), Southern California (blue), Bay Area (green), Central Valley (red), and Other (cyan). Southern California tracer is negligible at Walnut Grove. Assumed background of 120 ppb has been added to the tracers.

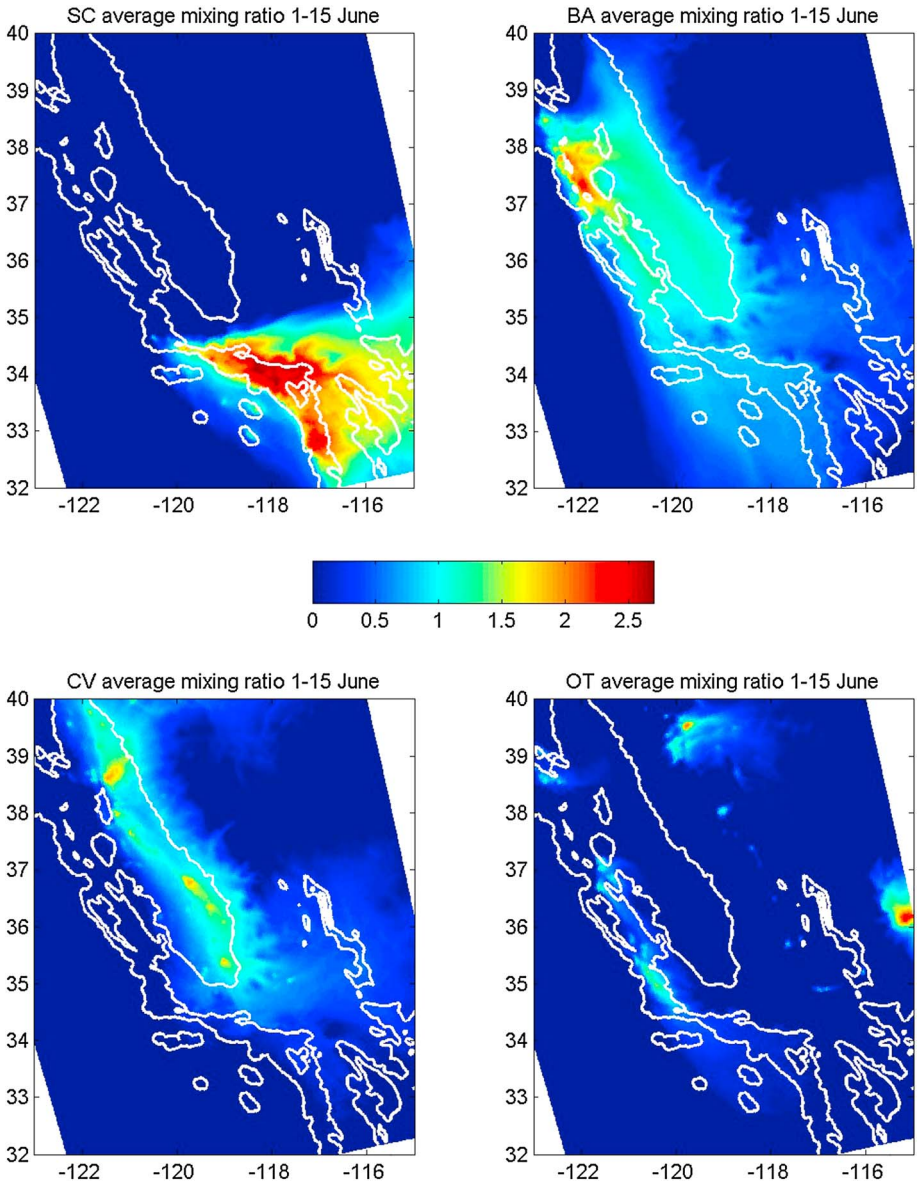

Figure 8. Average mixing ratios of each CO tracer (log10 (ppb)) in the lowest model layer for all hours of 1–15 June. Log (base 10) scale is used to make small concentrations visible. No background is added in this figure.

possibly coupled with errors in timing of boundary layer growth and restratification. The measurement is extremely variable during the times of greatest disagreement.

[15] Measurements of CO and other trace gases are conducted as part of the California Greenhouse Gas Emissions Measurement (CALGEM) project continuously at three levels (31, 91, and 483 m agl) on a tall tower (121.4911°W, 38.2650°N, 0 m above sea level (asl)) near Walnut Grove, California (WGC) in the Sacramento river delta [*Fischer et al.*, 2009; *Jeong et al.*, 2012]. Figure 6 shows the time series of measured CO (at 31 m agl) and simulated CO tracer at WGC. A diurnal pattern is visible, with considerable day-to-day variability. Measurements and model agree fairly well in some periods and not so well in others. The diurnal pattern is clearer in the simulation. The first of two large peaks on 14–15 June is well simulated, and the second peak is much too strong in the simulation. In the vertical (not shown), most of the CO tracer at WGC is below 500 m, and almost all of it is below 1 km. The average profile agrees reasonably well with the tower measurements (also not shown). The lower panel of the figure compares the simulated Bay Area CO tracer at WGC and Chowchilla, roughly halfway down the San Joaquin Valley. The diurnal pattern is also visible at Chowchilla, and some time lag can also be seen. More tracer at Chowchilla indicates that WGC is not precisely on the transport path between the Bay Area and the San Joaquin Valley. During 10–13 June, no Bay Area CO tracer reaches either site. All of the simulated CO in the upper part of the figure during those days comes from the Central Valley. The time series provide context for the average diurnal cycles shown in Figure 7. Here we also see that the diurnal cycle is larger and clearer in the simulation than in the measurements. Around midday, the variability (standard deviation) in the model and measurements is comparable, but in the morning the

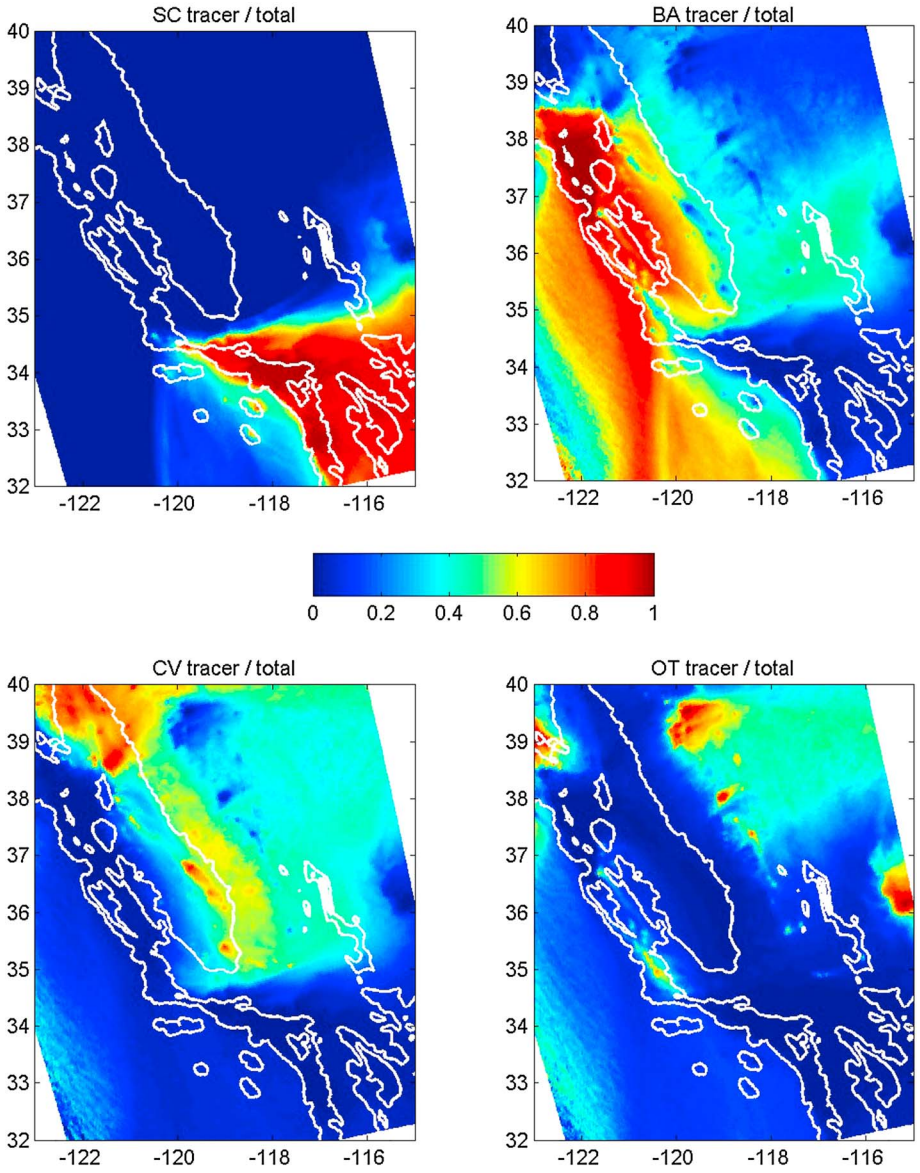

Figure 9. Ratios of CO regional tracers in the lowest model level for 1–15 June. Each tracer is summed over all hours and divided by the sum over all tracers and all hours.

measurements are much more variable. The Bay Area tracer is dominant except in the morning when the Central Valley tracer is at its maximum.

[16] Overall, the evaluation results we have shown indicate that we can have reasonable confidence in the simulations in the Los Angeles area, especially above the surface. A general overestimate of tracer relative to measured CO does not affect the results we will show below (see section 6). Fewer data exist for other regions, but what data we have indicate that the Bay Area CO tracer is probably reasonably well simulated, but we have less confidence in the Central Valley CO tracer, especially at the surface.

4. CO Tracer Age and Transport Among Regions

[17] With the caveats above in mind, we proceed to examine the simulations to learn how the tracers (simulated CO or NH_3 tagged by region and age) are transported among regions and how long it takes. We begin with maps of spatial patterns below. Several specific sites (see Figure 1) will also be shown to illustrate transport and aging. The 1–15 June period is used for these illustrations. This period had near average climatic conditions for that time of year [*Ryerson et al.*, 2013]. Compared to the whole CalNex period, 1–15 June was somewhat more polluted, but the basic patterns were similar (not shown).

[18] Figure 8 shows the simulated mean mixing ratio of each CO tracer, using a log scale so that small mixing ratios are visible. Contrasting this figure with Figure 2 shows the influence of transport beyond the areas with strong emissions. Transport pathways to the east and northeast from the Los Angeles area, and east and south from the Bay Area, are easily seen. On average, little of the Bay Area tracer is transported northeastward to the Sacramento Valley in this simulation. The Central Valley tracer influences areas to the east. Influence of the Other tracer is small in absolute terms

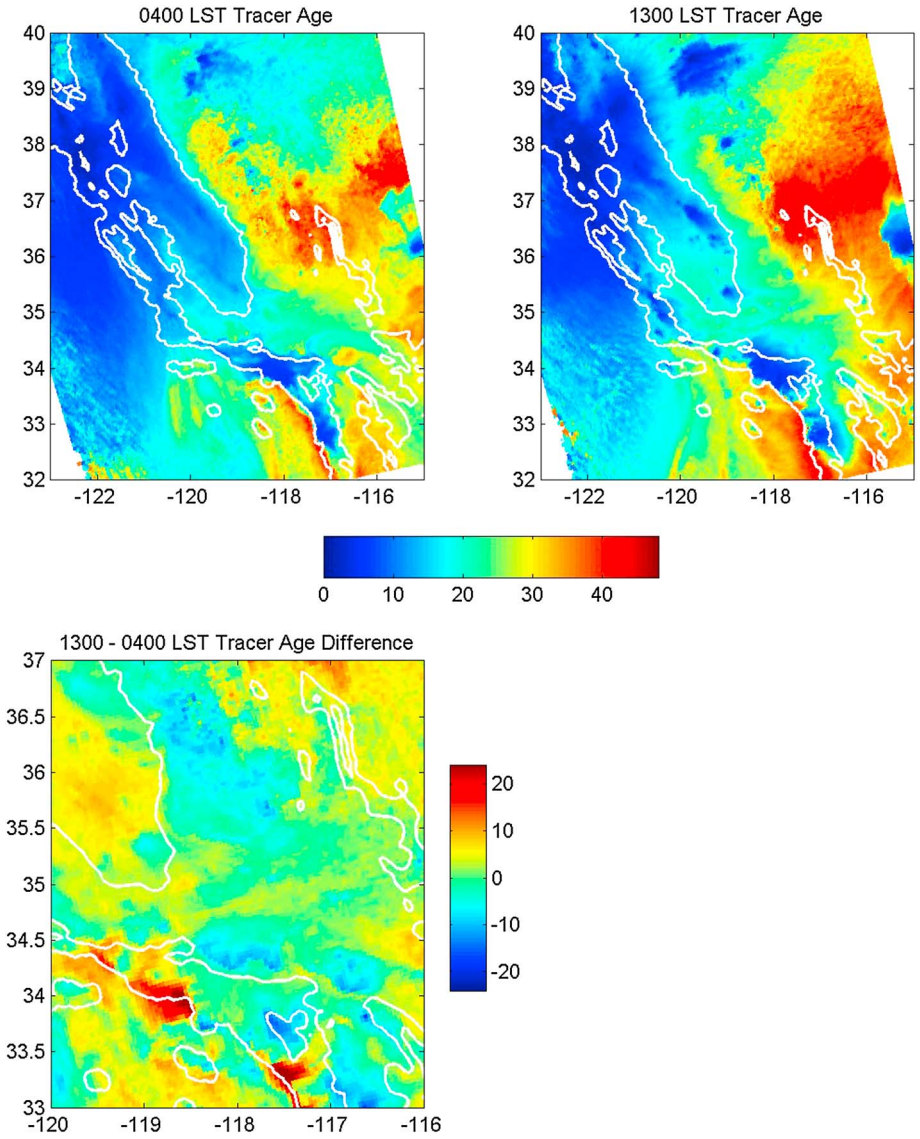

Figure 10. Average CO tracer age in the lowest model layer at 0400 LST and 1300 LST of 1–15 June (hours). Lower panel shows difference (hours) zoomed in on Southern California to show more detail.

except in the vicinity of Reno and Las Vegas, Nevada (not shown in these cropped plots).

[19] A complementary view is provided by the ratios of CO regional tracers (Figure 9). These show where the tracer present in a particular area came from, regardless of how much tracer is there. The Southern California tracer is confined entirely to Southern California, with no detectable influence north of the mountains that mark the northern edge of the Los Angeles basin, except very small ratios very far to the east. The Central Valley tracer has nearly no influence on Southern California or on the Bay Area but strong influence east and north of the area where it is emitted. The Other tracer influences areas near its emissions and east of the Sierra Nevada. It also has a small influence in ratio terms over the water. The most widely distributed tracer is from the Bay Area. It dominates over the water and the coast ranges south of the Bay. It also dominates the San Joaquin Valley except for those areas with their own strong emissions of the CV tracer. It does not, however, have much influence on the Sacramento Valley, which is dominated by the CV tracer, primarily local emissions from the city of Sacramento and its vicinity.

[20] Tracer age is a measure of travel time from emissions sources, integrated over the entire source area (Figure 10). The age patterns are broadly similar in the early morning and the early afternoon, with some interesting differences. Areas with strong emissions have primarily fresh tracer at all times, for example, most of the land area of Southern California west of −117° longitude, and the Bay Area. The southern San Joaquin Valley, except for the immediate vicinity of Bakersfield, has more aged tracer (20–24 h) in the afternoon, when local emissions have been transported to the east (upslope) and replaced by older tracer from the Bay Area. Over the water in the Southern California Bight, the tracer is aged, with older tracer to the east near shore. This is due to the "Catalina" eddy [*Angevine et al.*, 2012], which circulates aged Southern California emissions (seen as fresh tracer in Santa Monica Bay at 0400 local standard time LST) around and combines them with aged

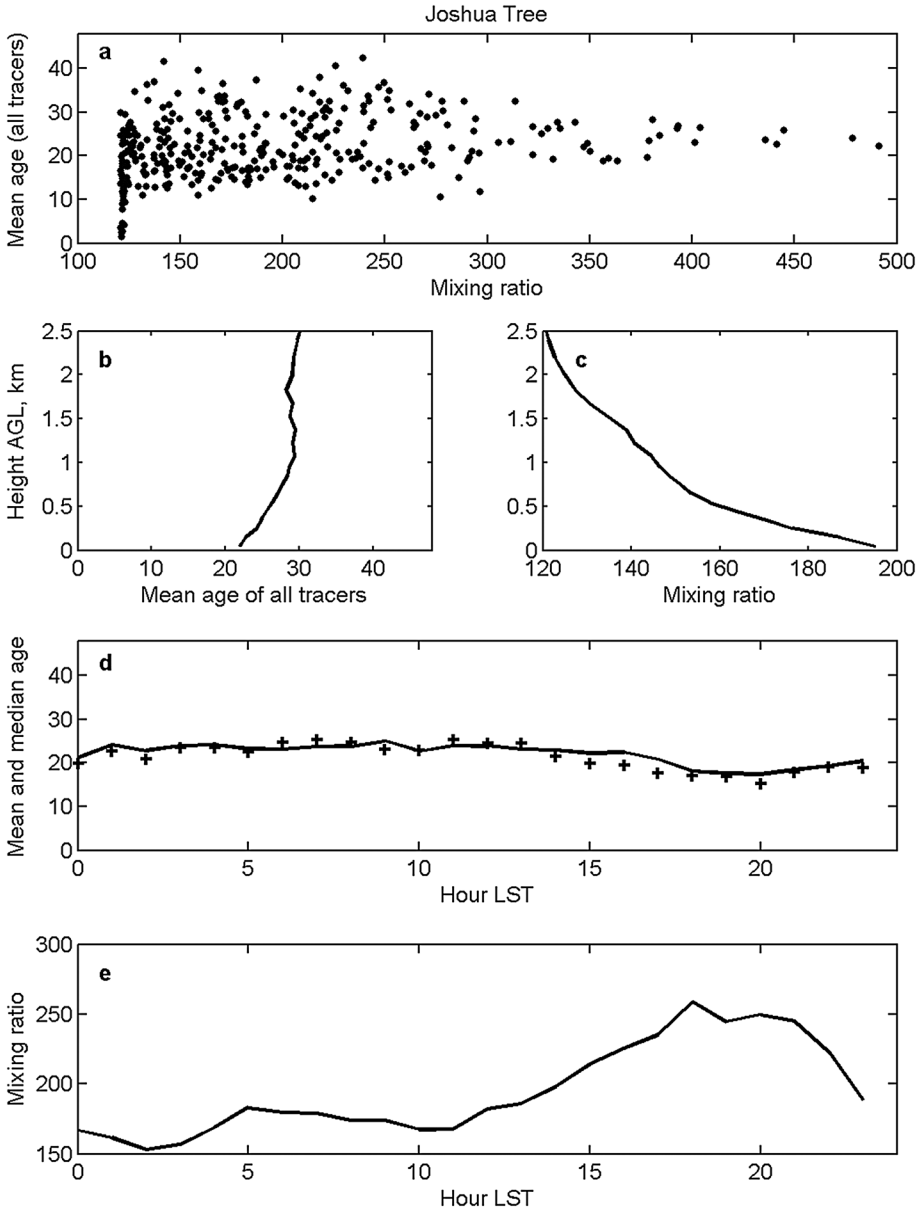

Figure 11. (a) CO tracer age (every hour) versus total mixing ratio (ppb) in the lowest FLEXPART level at Joshua Tree. (b) Mean age (hours) by height. (c) Mean mixing ratio of total CO tracer by height. For this site, essentially all the CO tracer is from Southern California. (d) CO tracer age in the lowest FLEXPART layer by time of day. (e) Mixing ratio of total CO tracer by time of day.

Bay Area emissions brought down the coast. For land areas, the pattern of tracer age is broadly similar to the ratio of fossil fuel CO_2 to local fossil fuel CO_2 emissions shown by *Riley et al*. [2008, Figure 6]. Both quantities are maximum where local emissions are weak and pollutants are transported from some distance.

[21] One of the most polluted periods during CalNex occurred on 4–5 June. Figures S1–S4 and Animations S5 and S6 in the supporting information show the evolution of CO tracer age, mixing ratio, and tracer ratios during that period. At 0700 LST on 4 June, Southern California and the Bay Area had large tracer mixing ratios, with moderate amounts of tracer in the Central Valley, desert, and a few other areas. The tracer in populated areas was mostly fresh, except for the southern San Joaquin Valley, where it was up to a day old, and the deserts, where it was as much as 36 h old. The influence of each of the areas, shown by the tracer ratios, was similar to the averages shown above. The broadest influence was from the Bay Area (Animation S5), which dominated most of the state north of the Los Angeles basin as well as the coastal waters including the western part of the Southern California Bight. The eastern Bight had areas of primarily SC tracer, but the area near shore in Orange County was primarily affected by tracer from the Bay Area. By 1300 LST, tracer mixing ratios had decreased in the areas of strongest emissions, due to increasing mixing heights. Onshore winds along the coast had pushed the tracer inland everywhere, and paths of tracer transport from the Bay Area into the interior were visible. What tracer was present along the Orange County coast was from Southern California.

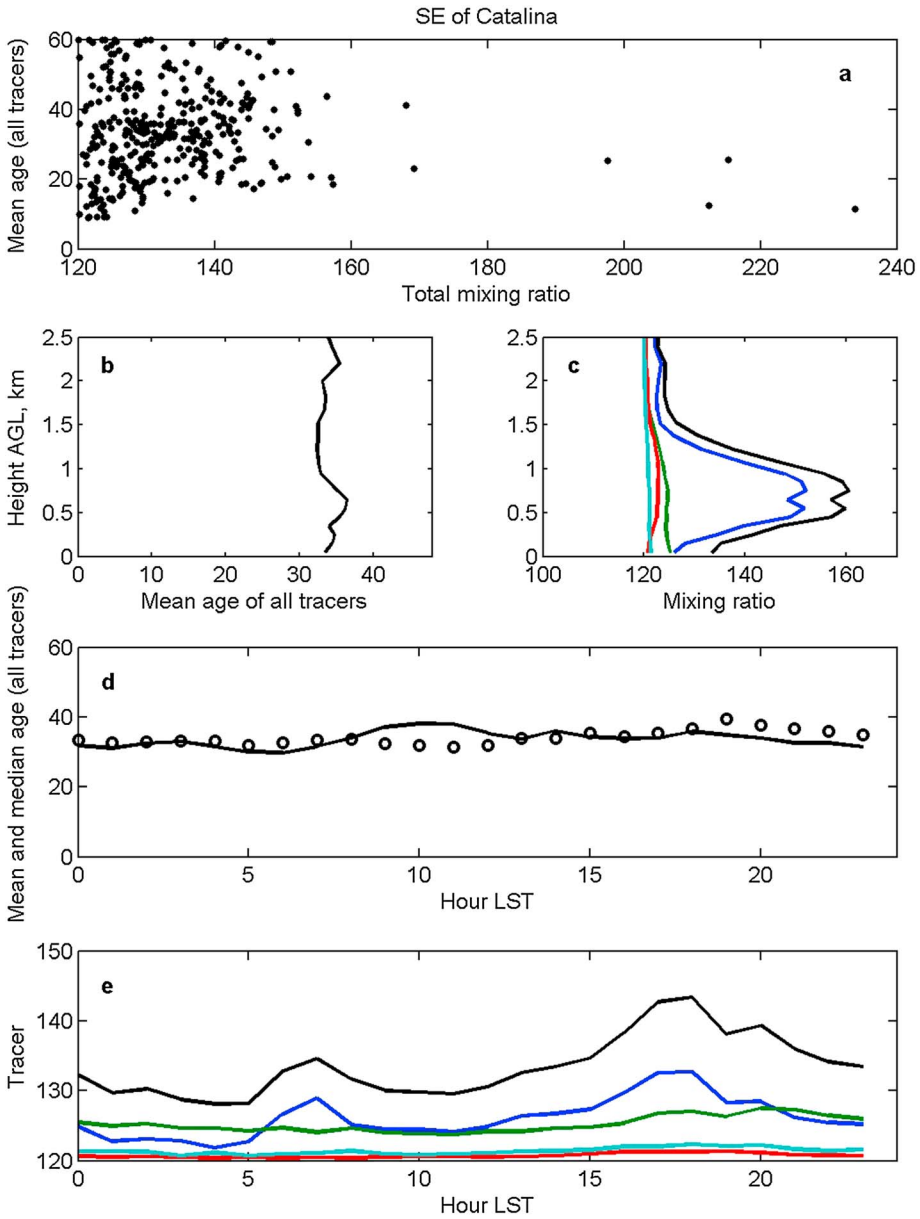

Figure 12. (a) CO tracer age (every hour) versus total mixing ratio (ppb) in the lowest FLEXPART layer at a point in the Southern California Bight southeast of Catalina Island. (b) Mean CO tracer age by height. (c) Mean mixing ratio of total (black) and each CO tracer by height. Tracers are Southern California (blue), Bay Area (green), Central Valley (red), and other (cyan). (d) CO tracer age in the lowest FLEXPART layer (solid) and at 950 m asl (circles) by time of day. (e) Mixing ratio of all (black) and each CO tracer by time of day. Tracers are Southern California (blue), Bay Area (green), Central Valley (red), and other (cyan).

[22] As the evolution continued, by 1900 LST in the evening, the southern San Joaquin Valley was dominated by local emissions (CV tracer) as the previous cycle's BA emissions had been transported away to the east. The Bight was filled with well-aged tracer mostly from the Bay Area. By shortly after midnight (0100 LST), the new pulse of Bay Area tracer had reached the south end of the San Joaquin Valley, and the day's CV emissions had moved south and east. The coastal waters were again populated by small amounts of tracer primarily from the Bay Area. The northern Bight had received SC tracer by way of the land breeze, and the Bay Area tracer dominated the Orange County coast again. The Bight also contained a contribution from the OT tracer, from sources along the coast north of Pt. Conception.

[23] The diurnal cycle of tracer at the Caltech ground site is shown in Figure 4. The tracer at Caltech is always less than 18 h old (not shown), and the mean age at the surface is about 8 h. Above 800 m agl, the age rapidly increases to a day or more, and total mixing ratio decreases quickly. In other words, the boundary layer at Caltech is populated by large concentrations of fresh emissions, with less and older tracer aloft.

[24] Joshua Tree National Park is east (downwind) of the Los Angeles metroplex, outside the basin. As shown in Figure 11, it receives tracer aged an average of nearly a day

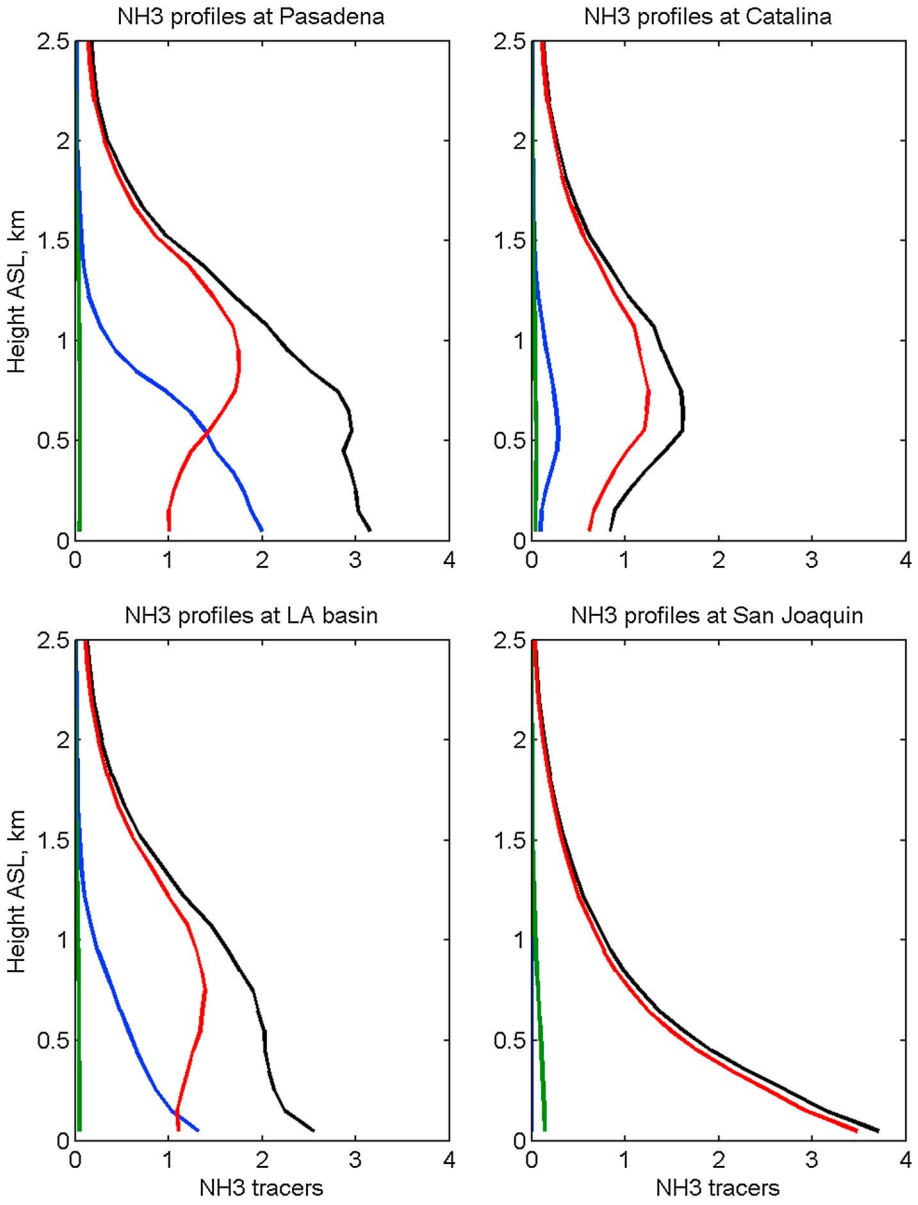

Figure 13. Average profiles of simulated agricultural tracer mixing ratios (ppb) for regions as defined for Figure 3 above. Total NH_3 tracer in black, SC NH_3 in blue, CV NH_3 in red, and BA NH_3 in green. OT tracer is negligible in all profiles.

at the surface, increasing to about 30 h aloft. The strongest mixing ratios at the surface are the same age as the average, about a day. Nearly all the tracer comes from Southern California. Average mixing ratios peak in the late afternoon and evening, and the tracer is slightly younger at those times but still most of a day old. In other words, on average, the afternoon peak concentrations at Joshua Tree were emitted on the previous day.

[25] One of the objectives of the CalNex campaign was to understand what role if any the air over the Southern California Bight (waters offshore of Southern California south of Pt. Conception) plays in transport and storage of pollution. In this respect the simulations show some interesting results. Figure 12 indicates that there are small but non-negligible levels of CO tracers from several regions over the Bight. In and above the marine boundary layer, most of the tracer is from Southern California, but at the surface there is an equal contribution from the Bay Area, brought down the coast by the persistent alongshore northwest winds. Tracer over the Bight is well aged at all heights. Age is broadly distributed and independent of mixing ratio. The diurnal cycle at the surface has distinct morning and afternoon peaks from Southern California. The Bay Area contribution is approximately constant through the day.

[26] At Bakersfield, in the southern San Joaquin Valley (previously shown in Figure 5), the CO tracer diurnal cycle peaks in the morning with a strong contribution from sources in the valley. There is also a contribution from the Bay Area, also peaking in the morning. The minimum local contribution corresponds to a maximum in tracer age. We recall that the simulated diurnal cycle at Bakersfield agrees poorly with the measured CO so some caution should be used in

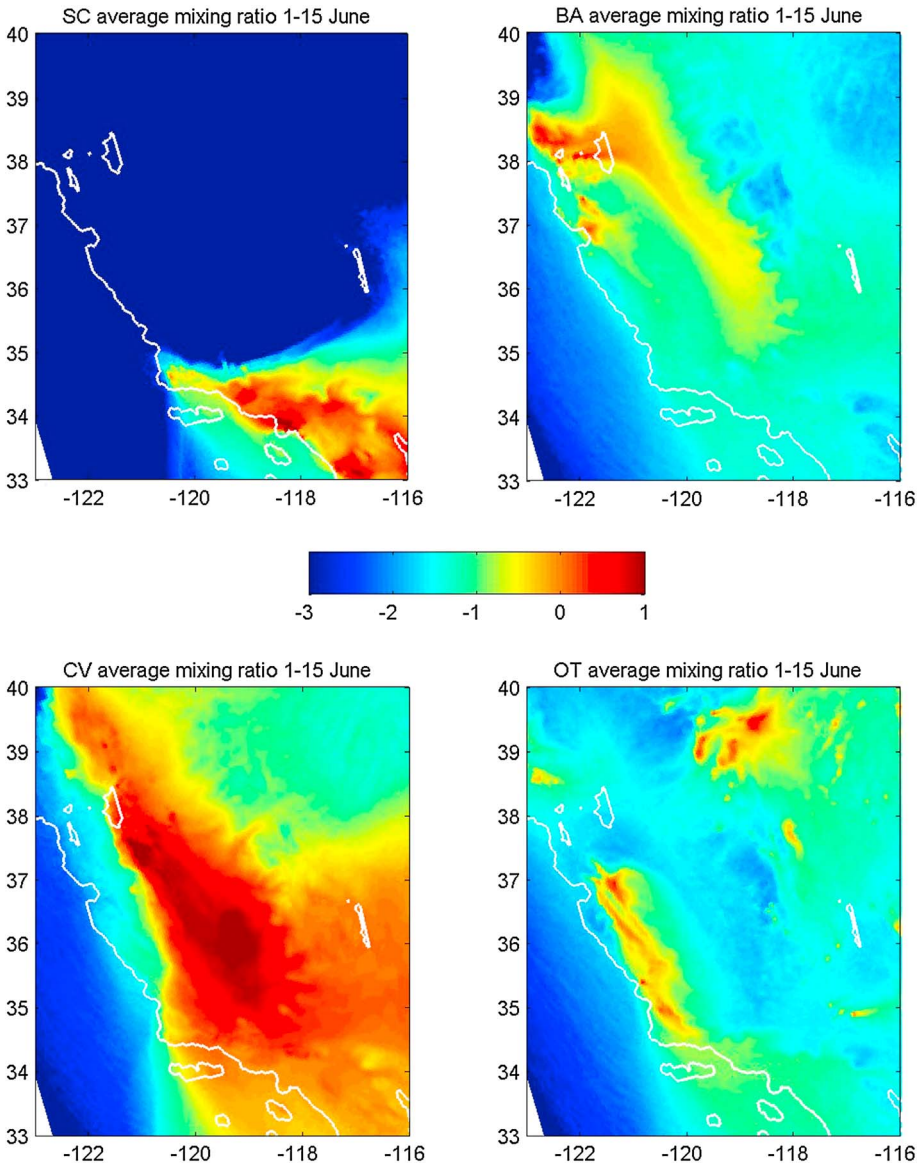

Figure 14. Mean agricultural tracer mixing ratios (log10(ppb)) in the lowest model layer for 1–15 June.

interpretation. The Central Valley contribution dominates the overall average below 500 m agl (not shown) but is the same size as the Bay Area contribution above 800 m.

5. Agricultural Tracer Results

[27] Simulations with the agricultural (NH_3) tracers show a different pattern than automotive CO because of the different spatial distribution of those emissions. Figure 2 shows the spatial pattern of NH_3 tracer emissions. Most of the emissions in the model are in the San Joaquin Valley. Compared to profiles measured by the P3 (not shown), the simulations have too little NH_3 at all heights except near the surface at Catalina and the LA basin. No background is added to the simulated NH_3 values, and deposition and conversion to the particle phase are not accounted for. The underestimate is consistent with the results of *Nowak et al.* [2012], who find large underestimates of NH_3 in the inventories. Leaving the magnitude aside and considering the NH_3 tracer only as a qualitative indicator of one type of agricultural emissions, we see (Figure 13) that Central Valley emissions account for nearly all of the tracer at Catalina, over the San Joaquin Valley (not surprising), and above 1 km over Pasadena and the broader LA basin. At Catalina, the NH_3 peak is above the marine boundary layer (500 m or shallower in the simulation). Southern California emissions account for about half of the total below 1 km over Pasadena and about one-third below 1 km over the LA basin. The NH_3 tracer concentrations are highly variable in time. At most locations, heights, and times of day, the temporal standard deviation is comparable to the mean, and diurnal cycles are weak compared to the day-to-day variability (not shown). In Figure 14, the total mixing ratio is largest in the San Joaquin Valley and Southern California, including the waters south of Pt. Conception (the Southern California Bight). In contrast to the automotive CO tracer, the NH_3 tracer over the Bight is almost entirely from the Central Valley. This reflects the difference in quantity and placement of emissions of CO versus NH_3. Automotive

CO emissions in the Central Valley are much smaller than in Southern California (Figure 2) and concentrated along the eastern edge of the valley, whereas the NH_3 emissions are greatest in the valley and quite widespread.

6. Uncertainty and Discussion

[28] Uncertainties exist in the simulations (and measurements) shown here, and it is not clear how to robustly estimate them. For this reason, the analysis and discussion here is in qualitative terms.

[29] Most likely, the uncertainty in the winds produced by WRF is important or even dominant. *Angevine et al*. [2012] compared those winds with a variety of measurements, but it is not obvious how to translate those comparisons into estimates of the uncertainty of the FLEXPART results. This question is discussed by *Vautard et al*. [2012]. A method of accounting for random wind errors in backward simulations at large scales is described in *Gerbig et al*. [2008] and *Lin and Gerbig* [2005]. This method requires estimates of the correlation scales of the wind errors and their magnitude. The correlation scales will vary strongly in space when simulated with grids on the order of 1 km in complex terrain, and measurements grossly undersample those scales, making estimates difficult.

[30] Vertical mixing of tracer in FLEXPART is another probably important source of uncertainty. The vertical profiles shown in Figure 3 indicate that the vertical structure of simulated tracer is quite reasonable. However, most of the other analyses use only the first model level (0–100 m agl), which is not accessed by the P3 profiles. The vertical profiles shown for other sites (Figures 11 and 12) indicate tracer mixing ratios increasing toward the surface except at the marine site (SE of Catalina), but in any case the profiles are smooth, so there is no indication of unrealistic trapping of emissions near the surface. *Gerbig et al*. [2008] suggest a method of accounting for errors in mixing height in large-scale backward simulations, but again, applying this method to our fine-scale simulations is not straightforward. The differing diurnal cycle between measurements and model at Bakersfield could be due to differences in timing of boundary layer growth and decay, but we cannot evaluate this further.

[31] Perhaps the most uncertain flows are those over the Southern California coast and waters. The land breeze, which transports tracer out to Santa Monica Bay, is weak in the simulations and in reality. *Angevine et al*. [2012] showed that different WRF configurations had different representations of the land-sea breeze circulation, all of which were somewhat flawed.

[32] Systematic errors (biases) in winds and vertical mixing are more important for our results than random errors. In forward simulations such as those shown here, failure to account for some random error means that the patterns we show will be sharper than in reality. Since the patterns are already rather smooth and dominated by terrain channeling, it seems unlikely that this is an important effect. Biases in the winds would shift the patterns in space and/or time. This remains, in our opinion, the largest uncertainty in the results. The known bias toward stronger winds will have the effect of decreasing concentrations in strong source regions and may increase concentrations in downwind areas (e.g., at Caltech, see Figure 4).

[33] Emissions are a third important source of uncertainty and of difficulty in estimating that uncertainty. It is not our purpose here to evaluate the emissions inventory, since we have more capable tools and analyses for that [*Brioude et al*., 2013]. The results here are sensitive to some aspects of emissions and not to others. Tracer ratios are sensitive to the relative amounts of tracer emitted in each region. Because the diurnal wind patterns interact with the emissions, tracer ages and ratios are sensitive to the diurnal cycle of emissions (e.g., Figure 4). The direct comparisons with measurements (e.g., Figures 3–7) are sensitive to the absolute amounts emitted. While not an uncertainty per se, it is important to keep in mind that the CO tracer simulates only light-duty on-road emissions. On the other hand, the light-duty on-road emissions and their diurnal cycle are the least uncertain of all types of emissions. The NH_3 tracer has quite a different spatial pattern of emissions, intended to represent some agricultural processes. Its absolute amount is uncertain and probably substantially underestimated [*Nowak et al*., 2012]. Transport of the NH_3 tracer results in quite different patterns of age and ratios from the CO tracer.

7. Conclusions

[34] The simulations of pollutant transport in May and June 2010 by the WRF/FLEXPART model system shown here conform to the basic picture built up over several decades of research (see references in section 1). Southern California emissions are transported to the east and affect the desert areas. Bay Area automobile emissions are an important source of pollutants in the San Joaquin Valley. Central Valley automobile emissions affect their local areas (e.g., Sacramento and Bakersfield) and the Sierra Nevada.

[35] We do see some novel, or at least easily visualized, results from the simulations, however. The Southern California Bight is filled with a mixture of aged CO tracer from Southern California and the Bay Area, with the two sources dominating at different times of day and locations within the Bight. The Bay Area tracer is transported down the coast by the prevailing northwesterly winds, introduced into the western edge of the Bight, and recirculated by the "Catalina" eddy. The Southern California tracer drifts out to Santa Monica Bay on the nocturnal land breeze and joins in the eddy circulation. Overall CO tracer mixing ratios are low. The fact that the air mass is aged is supported by hydrocarbon ratios measured on the ship (see Figure S7 and the accompanying discussion in the supporting information). Air over the Bight is also affected by the agricultural emissions represented by the NH_3 tracer, dominantly from the Central Valley where its sources are largest.

[36] In these simulations, there is no indication of transport from Southern California to the Central Valley. Emissions from the Central Valley do make their way to Southern California, as shown by the NH_3 tracer, but the contribution of automobile emissions in the Valley to Southern California is negligible because the Southern California automobile sources are so much larger. These results apply only to the time period we simulated (primarily early June) and probably to summer in general. Patterns in winter could be quite different.

[37] Future work in this area should include more precise estimates of uncertainty. Perhaps this could be done with well-designed ensembles of perturbed winds and/or emissions.

[38] **Acknowledgments.** The authors are grateful to Robert Harley for providing the diurnal cycle of CO and for helpful discussions. Andy Neuman provided helpful comments on the manuscript. We also wish to thank the NOAA P3 crew, flight planners, and scientists, and the crew and scientists of the R/V *Atlantis* CalNex cruise. The ERA-interim data used to initialize WRF are from the Research Data Archive (RDA), which is maintained by the Computational and Information Systems Laboratory (CISL) at the National Center for Atmospheric Research (NCAR). The original data are available from the RDA (http://dss.ucar.edu) in data set number ds627.0. Data collection at Walnut Grove was supported by NOAA and by the California Energy Commission (CEC) Public Interest Environmental Research Program and the Director, Office of Science, Office of Basic Energy Sciences, of the U.S. Department of Energy under contract DE-AC02-05CH11231.

References

Angevine, W. M., L. Eddington, K. Durkee, C. Fairall, L. Bianco, and J. Brioude (2012), Meteorological model evaluation for CalNex 2010, *Mon. Weather Rev.*, *140*, 3885–3906, doi:10.1175/MWR-D-12-00042.1.

Bao, J. W., S. A. Michelson, P. O. G. Persson, I. V. Djalalova, and J. M. Wilczak (2008), Observed and WRF-simulated low-level winds in a high-ozone episode during the Central California Ozone Study, *J. Appl. Meteorol. Clim.*, *47*(9), 2372–2394.

Beaver, S., and A. Palazoglu (2009), Influence of synoptic and mesoscale meteorology on ozone pollution potential for San Joaquin Valley of California, *Atmos. Environ.*, *43*(10), 1779–1788.

Brioude, J., et al. (2013), Top-down estimate of surface flux in the Los Angeles Basin using a mesoscale inverse modeling technique: assessing anthropogenic emissions of CO, NOx and CO_2 and their impacts, *Atmos. Chem. Phys.*, *13*, 3661–3677.

Brioude, J., et al. (2011), Top-down estimate of anthropogenic emission inventories and their interannual variability in Houston using a mesoscale inverse modeling technique, *J. Geophys. Res.*, *116*, D20305, doi:10.1029/2011JD016215.

Brioude, J., W. M. Angevine, S. A. McKeen, and E.-Y. Hsie (2012), Numerical uncertainty at mesoscale in a Lagrangian model in complex terrain, *Geosci. Model Dev.*, *5*, 1127–1136, doi:10.5194/gmd-5-1127-2012.

Chen, F., and J. Dudhia (2001), Coupling an advanced land surface-hydrology model with the Penn State-NCAR MM5 modeling system. Part II: Preliminary model validation, *Mon. Weather Rev.*, *129*, 587–604.

Chen, F., et al. (2011), The integrated WRF/urban modelling system: Development, evaluation, and applications to urban environmental problems, *Int. J. Climatol.*, *31*(2), 273–288.

Cooper, O. R., et al. (2011), Measurement of western U.S. baseline ozone from the surface to the tropopause and assessment of downwind impact regions, *J. Geophys. Res.*, *116*, D00V03, doi:10.1029/2011JD016095.

Dee, D. P., et al. (2011), The ERA-Interim reanalysis: Configuration and performance of the data assimilation system, *Q. J. R. Meteorol. Soc.*, *137*, 553–597.

Fast, J., and R. Easter (2006), A Lagrangian particle dispersion model compatible with WRF, paper presented at 7th WRF Users' Workshop, Natl. Cent. for Atmos. Res., Boulder, Colo., 19–22 June.

Fischer, M. L., C. Zhao, W. J. Riley, and A. C. Andrews (2009), Observation of CH4 and other non-CO_2 green house gas emissions from California *PIER Energy-Related Environ. Res., 500-2006-006*, Calif. Energy Comm., Sacramento.

Gerbig, C., S. Koerner, and J. C. Lin (2008), Vertical mixing in atmospheric tracer transport models: Error characterization and propagation, *Atmos. Chem. Phys.*, *8*, 591–602.

Harley, R. A., L. C. Marr, J. K. Lehner, and S. N. Giddings (2005), Changes in motor vehicle emissions on diurnal to decadal time scales and effects on atmospheric composition, *Environ. Sci. Technol.*, *39*, 5356–5362.

Janjic, Z. (2002), Nonsingular implementation of the Mellor-Yamada level 2.5 scheme in the NCEP meso model, *NCEP Off. Note 437*, 60 pp., Natl. Cent. for Environ. Predict., College Park, Md.

Jeong, S., C. Zhao, A. C. Andrews, L. Bianco, J. M. Wilczak, and M. L. Fischer (2012), Seasonal variation of CH4 emissions from central California, *J. Geophys. Res.*, *117*, D11306, doi:10.1029/2011JD016896.

Kim, S.-W., et al. (2011), Evaluations of NOx and highly reactive VOC emission inventories in Texas and their implications for ozone plume simulations during the Texas Air Quality Study 2006, *Atmos. Chem. Phys.*, *11*(22), 11361–11386.

Langford, A. O., C. J. Senff, R. J. Alvarez II, R. M. Banta, and R. M. Hardesty (2010), Long-range transport of ozone from the Los Angeles Basin: A case study, *Geophys. Res. Lett.*, *37*, L06807, doi:10.1029/2010GL042507.

Langford, A. O., J. Brioude, O. R. Cooper, C. J. Senff, R. J. Alvarez, II, R. M. Hardesty, B. J. Johnson, and S. J. Oltmans (2012), Stratospheric influence on surface ozone in the Los Angeles area during late spring and early summer of 2010, *J. Geophys. Res.*, *117*, D00V06, doi:10.1029/2011JD016766.

Lin, J. C., and C. Gerbig (2005), Accounting for the effect of transport errors on tracer inversions, *Geophys. Res. Lett.*, *32*, L01802, doi:10.1029/2004GL021127.

Michelson, S. A., and J.-W. Bao (2008), Sensitivity of low-level winds simulated by the WRF model in California's Central Valley to uncertainties in the large-scale forcing and soil initialization, *J. Appl. Meteorol. Clim.*, *47*, 3131–3149.

Neuman, J. A., et al. (2012), Observations of ozone transport from the free troposphere to the Los Angeles basin, *J. Geophys. Res.*, *117*, D00V09, doi:10.1029/2011JD016919.

Nowak, J. B., J. A. Neumann, R. Bahreini, A. M. Middlebrook, J. S. Holloway, S. A. McKeen, D. D. Parrish, T. B. Ryerson, and M. Trainer (2012), Ammonia sources in the California South Coast Air Basin and the impact on ammonium nitrate formation, *Geophys. Res. Lett.*, *39*, L07804, doi:10.1029/2012GL051197.

Pfister, G. G., J. Avise, C. Wiedinmyer, D. P. Edwards, L. K. Emmons, G. D. Diskin, J. Podolske, and A. Wisthaler (2011), CO source contribution analysis for California during ARCTAS-CARB, *Atmos. Chem. Phys.*, *11*, 7515–7532.

Riley, W. J., D. Y. Hsueh, J. T. Randerson, M. L. Fischer, J. G. Hatch, D. E. Pataki, W. Wang, and M. L. Goulden (2008), Where do fossil fuel carbon dioxide emissions from California go? An analysis based on radiocarbon observations and an atmospheric transport model, *J. Geophys. Res.*, *113*, G04002, doi:10.1029/2007JG000625.

Ryerson, T. B., et al. (2013), Overview of the 2010 California Research at the Nexus of Air Quality and Climate Change (CalNex) field study, *J. Geophys. Res. Atmos.*, doi:10.1002/jgrd.50331, in press.

Skamarock, W. C., J. B. Klemp, J. Dudhia, D. O. Gill, D. M. Barker, M. G. Duda, X.-Y. Huang, W. Wang, and J. G. Powers (2008), A description of the Advanced Research WRF version 3, *NCAR Tech. Note TN-475*, 113 pp., Natl. Cent. for Atmos. Res., Boulder, Colo.

Stohl, A., C. Forster, A. Frank, P. Seibert, and G. Wotawa (2005), Technical note: The Lagrangian particle dispersion model FLEXPART version 6.2, *Atmos. Chem. Phys.*, *5*, 2461–2474.

Sušelj, K., and A. Sood (2010), Improving the Mellor–Yamada–Janjić parameterization for wind conditions in the marine planetary boundary layer, *Boundary Layer Meteorol.*, *136*, 301–324.

US Environmental Protection Agency (2012), 2005 National Emissions Inventory Data & Documentation available at http://www.epa.gov/ttnchie1/net/2005inventory.html.

Vautard, R., et al. (2012), Evaluation of the meteorological forcing used for the Air Quality Model Evaluation International Initiative (AQMEII) air quality simulations, *Atmos. Environ.*, *53*(0), 15–37.

White, W. H., and E. S. Macias (1990), Regional transport of the urban workweek: Methylchloroform cycles in the Nevada-Arizona desert, *Geophys. Res. Lett.*, *17*, 1081–1084, doi:10.1029/GL017i008p01081.